WOOD RESEARCH doi.org/10.37763/wr.1336-4561/67.6.979993
e-ISSN 2729-8906
67(6): 2022 979-993 pp.

MODELLING FOR SINGLE-WALL CORRUGATED FIBREBOARD WITH A TRAPEZOIDAL CORE UNDER THE QUASI-STATIC EDGEWISE CRUSHING LOAD

GUAN SHILI, LIANG YOUZHEN, WANG JUN, LU LIXIN
JIANGNAN UNIVERSITY
CHINA

HOU XUE
WUXI INNOVATION RESEARCH INSTITUTE OF SHANTOU DONGFENG PRINTING CORPORATION
CHINA

(RECEIVED MAY 2022)

ABSTRACT

In this paper, the energy absorption of single-wall corrugated fibreboard with a trapezoidal core under edgewise crushing load was studied experimentally and analytically, and a physical surface bonding was assumed to represent the interaction between the fluted board and the linerboard based on the production process of corrugated fibreboards. A new folding element was proposed, including two boards and two trapezoidal corrugated cores with central symmetry. Moreover, three folding modes of the fluted board were proposed based on experimental phenomena, and a plateau stress model was characterized by the geometry parameters of the corrugated fibreboard. It was found that the plateau stress predicted by the developed model compared well with the experimental results, from which one can conclude that the proposed model was effective and helpful for corrugated structures design and parameters selection to meet different strength requirements.

KEYWORDS: Single-wall corrugated fibreboard, trapezoidal core, edgewise crushing load, plateau stress, energy absorption.

INTRODUCTION

Thin-walled multi-cell structures, such as corrugated fibreboards, were widely used in transport packaging, aerospace, and other fields due to their excellent cushioning energy

absorption and compression performance, and the energy absorption behavior of which received a lot of attention (Russ et al. 2013, Duan et al. 2019, Gao and Liao 2021). Corrugated fibreboards are a widely applied kind of thin-walled multi-cell structures and good candidates for energy absorption in real engineering applications, which are mainly subjected to out-of-plane loading (Fig. 1, loading in the thickness direction) and in-plane loading (Fig. 1, loading in the machine direction or cross direction).

Previous research mainly focused on the performance of the corrugated structure under the external force acting on the thickness direction (Zhang et al. 2019, Garbowski et al. 2021, Yu-Ping and Wang 2012). However, the edgewise compression (external force acts on the cross direction) was also the common loading condition in the distribution process (Kolakowski et al. 2015), during which the corrugated fibreboard will usually be folded progressively. There is a long plateau stage in the stress-strain curve of a corrugated fibreboard under edgewise crushing load which is depicted in Fig. 2. It is of great importance to reveal the mechanism for the mechanical behavior of corrugated fibreboard for structure design. However, the past studies were mainly based on experiment or simulation results (Westerlind and Carlsson 1992, Szewczyk and Bienkowska 2020, Jamsari et al. 2020). In recent years, based on Super Folding Element (SFE) theory (Wierzbicki 1983) and Simplified Super Folding Element (SSFE) theory (Chen and Wierzbicki 2001), Li et al. 2018 studied the plateau stress model of corrugated fibreboard under quasi-static edgewise crushing load and then extended the plateau stress model for the multi-layer corrugated fibreboard. Most recently, this group further proposed a typical folding element and plateau stress model (Bai et al. 2019) for the corrugated fibreboards based on Zhang X's angle elements theory (Zhang and Zhang 2013), which was found to be more accurate.

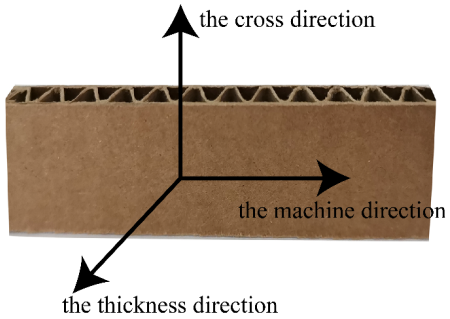

Fig. 1: Structure diagram of corrugated fibreboard.

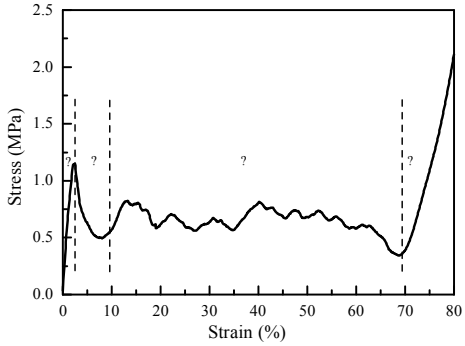

Fig. 2: Typical stress-strain curve of the corrugated fibreboard under edgewise crushing load.

For nearly all published research, the shape of corrugated fibreboard core was generally regarded as triangular, which is actually bonded by a trapezoidal interface. The present work aims to extend our group's previous research to the quasi-static model for corrugated fibreboards with a trapezoidal core. A new folding element is proposed firstly, and three deformation modes of the corrugated core are proposed. Then, a theoretical model for corrugated fibreboard with a trapezoidal core under edgewise crushing load is derived and verified experimentally. Therefore, the key to this paper is extending the knowledge into the mechanical models of the plateau stress instead of based on the experimental studies, which have promising applications in designing the corrugated containers and characterizing the energy

absorption properties of the corrugated paperboards in an actual logistic environment.

Typical folding element selection

Structurally, the single-wall corrugated fibreboard with a trapezoidal core is composed of a linerboard I, a fluted board, and a linerboard II. The corrugated fibreboard structure under the overall edgewise crushing load can be reflected by the local folding element, in which the continuous corrugated shape is repeated to form the corrugated fluted board. The corrugated shape can generally be simplified to a sine curve (Aboura et al. 2004), cosine curve (Isaksson et al. 2007), trapezoid (Moon et al. 2009), triangle (Buannic et al. 2003), or tangent arc (Urbanik 2001).

However, in the case of an actual corrugated fibreboard, the bonding process, cots, and pressure rollers would flatten the original corrugated curve. Therefore, surface bonding was assumed to represent the interaction between the fluted board and the linerboard (Fig. 3). Based on this assumption, the corrugated shape was close to a trapezoid, but the connection between the collapsed part of the corrugated top and the inclined straight line was smooth. Zhang and Zhang (2013) reported that the influence of the arc at the joint was negligibly small. In this study, the following point of view is put forth: for a fluted board, a simplified model with a trapezoidal core can be used to not only simplify the calculation but also ensure the accuracy of the model.

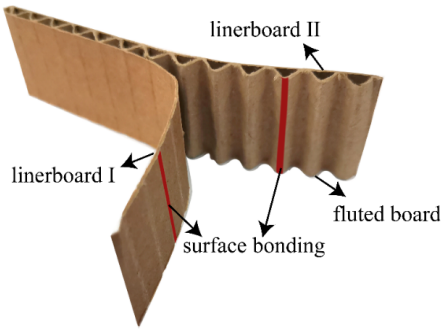

Fig. 3: Assuming that the interaction was surface bonding.

The typical folding elements of corrugated fibreboards should follow two principles (Bai et al. 2019): *(1)* the typical folding elements cannot be intercepted from the corner; *(2)* the typical folding elements can be used to represent the overall structure. In this light, the process of selection of the typical folding elements followed herein is illustrated in Fig. 4. Then the selection of the typical folding elements consisted of the AB part of the linerboard Ⅰ, the CD part of the linerboard Ⅱ, and two trapezoids with the central symmetry of the fluted board.

(a)

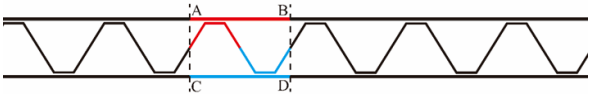

(b)

Fig. 4: The typical folding element of (a) corrugated fibreboard (b) simplified model.

Fig. 5 illustrates the typical folding element dimensions of the corrugated fibreboard, where the length of the typical folding element length is denoted by λ and the length of the bonding part by h. The wall length is l, and the angle between the fluted board and the linerboard is θ. In addition, the thicknesses of the linerboard I, fluted board, and linerboard II as the corrugated fibreboard raw materials are t_1, t_0, and t_2, respectively, and the overall thickness of the corrugated fibreboard is T.

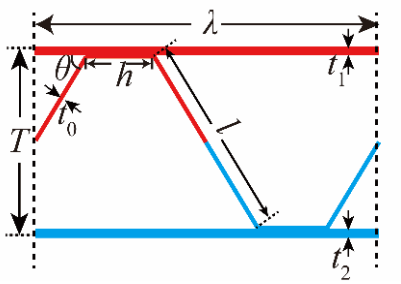

Fig. 5: Dimensions of the typical folding element.

Deformation mode

Folding of the fluted board would lead to simultaneous bending of the linerboard. This effect of the fluted board on the linerboard was termed the "induced effect" (Bai et al. 2019). As shown in Fig. 6, the linerboard I and the linerboard II underwent bending deformation only. Therefore, in the present research, the focus is on the deformation mode of the fluted board.

Fig. 6: Deformation mode of the linerboard.

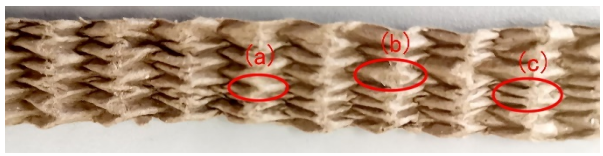

Fig. 7: Deformation mode of the fluted board.

The typical folding element selection of the fluted board was composed of two trapezoidal elements with central symmetry (Fig. 9). Therefore, to analyse the deformation mode of the fluted board, only one trapezoidal element needs to be studied. Fig. 7 shows the deformation mode of the fluted board in the edgewise compression test, where three deformation modes existed. Fig. 8 shows the folding elements corresponding to these three deformation modes: the symmetric mode, the outer folding mode and the inner folding mode, respectively.

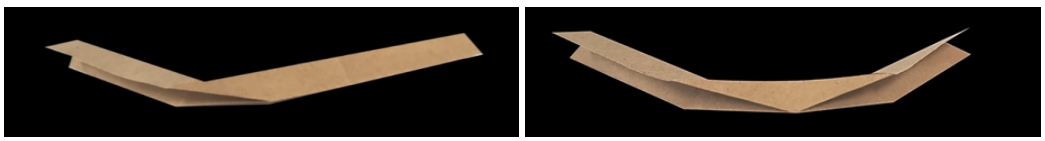

(a) Asymmetric mode.

(b) Outer folding mode.

(c) Inner folding mode.

Fig. 8: Deformation mode of the folding elements.

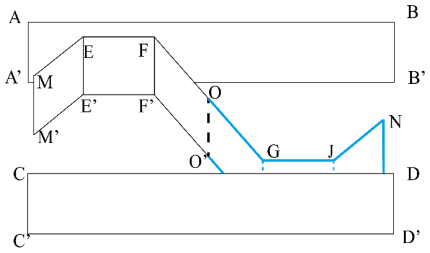

Fig. 9: Three-dimensional diagram of the typical folding element.

Fan et al. (2013) and Wang et al. (2018) demonstrated that different deformation modes are accompanied by different tension and compression areas, which would lead to different plateau stresses. As shown in Fig. 10, the rolling area of membrane deformation in the asymmetric mode can be expressed as follows:

$$\Delta S_{asy} = H^2 \cot\frac{\theta}{2} \tag{1}$$

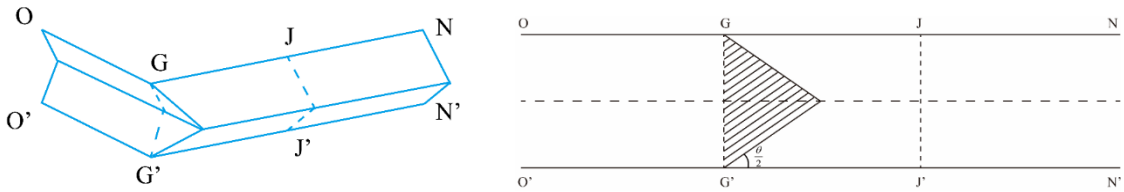

(a) Three-dimensional diagram. (b) Unfold diagram.

Fig. 10: Asymmetric mode.

As shown in Fig. 11, the rolling area of membrane deformation in the outer folding mode can be expressed as follows:

$$\Delta S_{outer} = H^2 \tan\frac{\theta}{2} \tag{2}$$

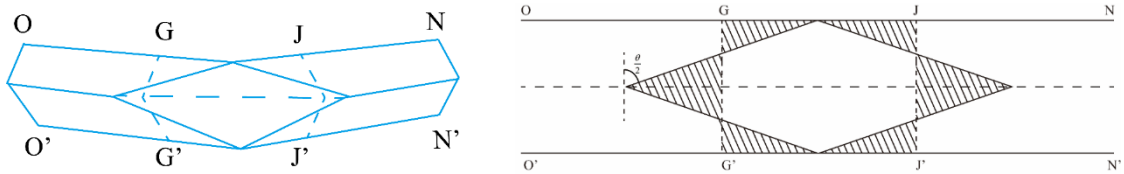

(a) Three-dimensional diagram. (b) Unfold diagram.

Fig. 11: Outer folding mode.

As shown in Fig. 12, the rolling area of membrane deformation in the inner folding mode can be expressed as follows:

$$\Delta S_{inner}=2H^2\cot\frac{\theta}{2} \tag{3}$$

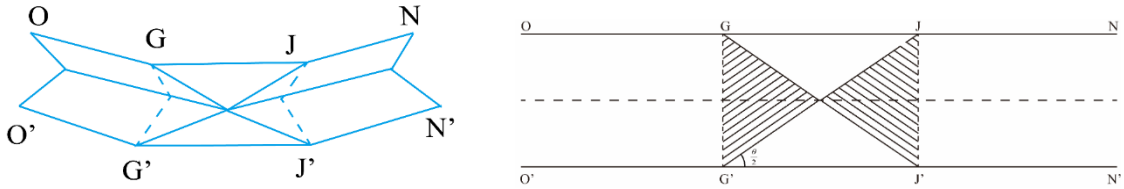

(a) Three-dimensional diagram. (b) Unfold diagram.

Fig. 12: Inner folding mode.

Calculation of energy dissipation

Three classical theories are available to describe energy absorption in thin-walled structures: SFE (Wierzbicki 1983), SSFE[25] (Chen and Wierzbicki 2001), and Zhang X's angle element theory (Zhang and Zhang 2013). The results of the last one illustrated that the average edgewise crushing force and energy absorption of multi-element columns and three plate angle elements could be extended to analyse any angular element. Therefore, the theoretical analysis was based on Zhang X's angle element theory.

By considering the energy equilibrium, the work done by the mean crushing force in one folding wavelength $2H$ was equated to the amount of energy dissipated internally, as follows:

$$P_m\times 2H\cdot k=W \tag{4}$$

where: P_m denotes the mean crushing force acting during the collapse of a typical folding element, $2H$ is the folding wavelength, k is the coefficient of effective crushing distance, and W represents the amount of energy dissipated internally:

$$W=W_1+W_0+W_2 \tag{5}$$

where: W_1, W_2 and W_3 denote the energies dissipated in the linerboard Ⅰ, fluted board, and linerboard Ⅱ, respectively.

The bending energy dissipation of one panel is:

$$W=\sum_{i=1}^{5} M\theta_i C \tag{6}$$

with

$$M=\frac{1}{4}\sigma_0 t_0^2 \tag{7}$$

where: M represents the fully plastic bending moment per element length, θ_i is the bending angle, and C is the length of the hinge line. In this paper, the length of the hinge line of the linerboard is λ. Additionally, σ_0 and t represent flow stress and material thickness, respectively, and the value of flow stress is 0.92 times the value of ultimate stress σ_u (Abramowitz and Wierzbicki 1989).

Notably, the linerboard Ⅰ and the linerboard Ⅱ will be bent owing to the induced effect of the fluted board, as follows:

$$W_1 = 4\pi M_1 \lambda \quad (8)$$

$$W_2 = 4\pi M_2 \lambda \quad (9)$$

where: M_1 and M_2 represent the plastic bending moment per element length of the linerboard Ⅰ and the linerboard Ⅱ, respectively.

As illustrated by the blue part in Fig. 9, a typical folding element of the fluted board consists of two trapezoidal elements, which exhibit central symmetry. According to Zhang and Zhang 2013, the energy dissipated by one trapezoidal element can be divided into two parts: bending energy W_b of the static hinge line and overall rolling energy W_r of the hinge line, as follows:

$$W_{\text{half-0}} = W_b + W_r \quad (10)$$

The length of the hinge line of the fluted board is $(l+h)$, so the bending energy of static stranded wire is $2\pi M_0 (l+h)$. In fact, the bending energy is doubled due to complex reasons (Wierzbicki 1983, Zhang and Zhang 2013). Therefore, half of the bending energy of the fluted board is based on the plastic deformation process of the structure, a different explanation for the double bending energy was proposed recently by Zhang and Zhang 2013. Nevertheless, half of the bending energy of the fluted board certainly is:

$$W_b = 4\pi M_0 (l+h) \quad (11)$$

As for the overall rolling energy of the movable hinge line W_r', It includes the rolling energy dissipation W_r of the moving hinge line and the energy consumption W_m due to the deformation of the membrane. In this paper, $W_m = \int_{\Delta S} \sigma_0 t_0 ds = \frac{4M_0 \Delta S}{t_0}$ and $W_r = \frac{2M_0 \Delta S}{r}$. Therefore, it can be integrated as follows:

$$W_r' = \frac{2M_0 \Delta S}{r'} \quad (12)$$

with

$$r'(\theta) = 0.082 \left(\frac{l+h}{4}\right)^{0.6} t_0^{0.4} \left(\tan\frac{\theta}{2} + \frac{0.06}{\tan\frac{\theta}{2}}\right) \quad (13)$$

where: W_b represents the energy dissipation due to plastic deformation of the fluted board under bending, W_r' represents the energy dissipation due to plastic deformation of the fluted board under rolling, and $r'(\theta)$ denotes the integrated rolling radius of a folding element in the fluted board.

By substituting Eq. 1 and Eq. 11 into Eq. 10 and then substituting Eq. 10 and Eq. 9 into Eq. 8, we obtain the following expression:

$$W_{\text{half-0}}=W_b+W_r=4\pi M_0(l+h)+\frac{2M_0H^2\cot\frac{\theta}{2}}{r} \tag{14}$$

Therefore,

$$W_0=2W_{\text{half-0}}=8\pi M_0(l+h)+\frac{4M_0H^2\cot\frac{\theta}{2}}{r} \tag{15}$$

The internal energy dissipation in the asymmetric mode is defined as W_{asy}, and the mean crushing force in the asymmetric mode is defined as P_{asy}. By substituting Eqs. 8 and 9, and Eq.15 into Eq. 5, the following expression is obtained:

$$W_{\text{asy}}=W_1+W_0+W_2=4\pi M_1\lambda+8\pi M_0(l+h)+\frac{4M_0H^2\cot\frac{\theta}{2}}{r}+4\pi M_2\lambda \tag{16}$$

By substituting Eq. 16 into Eq. 4, the following equation is obtained:

$$\frac{P_{\text{asy}}\times k}{M_0}=\frac{4\pi(l+h)}{H}+\frac{2H^2\cot\frac{\theta}{2}}{r}+\frac{2\pi\lambda}{H}\left(\frac{M_1}{M_0}+\frac{M_2}{M_0}\right) \tag{17}$$

The folding half-wavelength H can be determined based on the stationary condition of the mean crushing force, as follows:

$$\frac{\partial P_{\text{asy}}}{\partial H}=0 \tag{18}$$

Therefore,

$$H=\sqrt{\frac{\pi\left[2l+2h+\left(\frac{M_1}{M_0}+\frac{M_2}{M_0}\right)\lambda\right]r}{\cot\frac{\theta}{2}}} \tag{19}$$

Assuming that $\frac{M_1}{M_0}=a$, $\frac{M_2}{M_0}=b$, and substituting Eq. 19 into Eq. 17, the mean crushing force of a typical folding element in the asymmetric mode can be expressed as follows:

$$P_{\text{asy}}=\frac{4M_0}{k}\cdot\sqrt{\frac{\pi[2l+2h+(a+b)\lambda]\cot\frac{\theta}{2}}{r}}=\frac{\sigma_0 t_0^2}{k}[2l+2h+(a+b)\lambda]^{\frac{1}{2}}\sqrt{\frac{\pi\cot\frac{\theta}{2}}{r}} \tag{20}$$

By using a similar analysis method, the mean crushing force of a typical folding element in the outer folding mode can be expressed as follows:

$$P_{\text{outer}}=\frac{4M_0}{k}\cdot\sqrt{\frac{\pi[2l+2h+(a+b)\lambda]\tan\frac{\theta}{2}}{r}}=\frac{\sigma_0 t_0^2}{k}[2l+2h+(a+b)\lambda]^{\frac{1}{2}}\sqrt{\frac{\pi\tan\frac{\theta}{2}}{r}} \tag{21}$$

The mean crushing force of a typical folding element in the inner folding mode can be expressed as follows:

$$P_{\text{asy}}=\frac{4M_0}{k}\cdot\sqrt{\frac{2\pi[2l+2h+(a+b)\lambda]\cot\frac{\theta}{2}}{r}}=\frac{\sigma_0 t_0^2}{k}[2l+2h+(a+b)\lambda]^{\frac{1}{2}}\sqrt{\frac{2\pi\cot\frac{\theta}{2}}{r}} \tag{22}$$

Plateau stress

The plateau stress σ is equal to P_m divided by the area of a typical folding element section, and therefore, it can be expressed as follows:

$$\sigma_{asy}=\frac{P_{asy}}{\lambda T}=\frac{\sigma_0 t_0^2}{k\lambda T}\cdot[2l+2h+(a+b)\lambda]^{\frac{1}{2}}\cdot\sqrt{\frac{\pi\cot\frac{\theta}{2}}{r}} \quad (23)$$

$$\sigma_{outer}=\frac{P_{outer}}{\lambda T}=\frac{\sigma_0 t_0^2}{k\lambda T}\cdot[2l+2h+(a+b)\lambda]^{\frac{1}{2}}\cdot\sqrt{\frac{\pi\tan\frac{\theta}{2}}{r}} \quad (24)$$

$$\sigma_{inner}=\frac{P_{inner}}{\lambda T}=\frac{\sigma_0 t_0^2}{k\lambda T}\cdot[2l+2h+(a+b)\lambda]^{\frac{1}{2}}\cdot\sqrt{\frac{2\pi\cot\frac{\theta}{2}}{r}} \quad (25)$$

where: σ_{asy}, σ_{outer}, and σ_{inner} represent the plateau stresses of the asymmetric mode, outer folding mode, and inner folding mode, respectively.

To obtain the plateau stress of the corrugated fibreboard, the three deformation modes can be added after multiplying them with suitable proportionality coefficients, as follows:

$$\sigma=x\cdot\sigma_{asy}+y\cdot\sigma_{outer}+z\cdot\sigma_{inner} \quad (26)$$

Therefore, the plateau stress associated with the corrugated fibreboard under quasi-static edgewise crushing can be expressed as follows:

$$\sigma=\frac{\sigma_0 t_0^2}{k\lambda T}\cdot[2l+2h+(a+b)\lambda]^{\frac{1}{2}}\cdot(x\cdot\sqrt{\frac{\pi\cot\frac{\theta}{2}}{r}}+y\cdot\sqrt{\frac{\pi\tan\frac{\theta}{2}}{r}}+z\cdot\sqrt{\frac{2\pi\cot\frac{\theta}{2}}{r}}) \quad (27)$$

MATERIALS AND METHODS

To study the accuracy of the plateau stress prediction model for single-wall corrugated fibreboard with a trapezoidal core, three types of single-wall corrugated fibreboards were selected for experimental verification. These corrugated fibreboards were supplied by Tat Seng-Packaging (Suzhou China). The structural parameters of the specimens are listed in Tab. 1.

Tab. 1: Parameters of the corrugated fibreboard specimens (according to Fig. 5).

Specimens	Ration ($g \cdot m^{-2}$)	λ (mm)	l (mm)	h (mm)	θ (°)	t_0 (mm)	t_1 (mm)	t_2 (mm)	T (mm)
A	120/110/120	8.00	4.00	2.00	60	0.228	0.180	0.180	4.050
C	170/160/170	7.50	3.20	2.15	60	0.256	0.222	0.222	3.770
C	230/130/150	7.60	3.80	1.90	60	0.231	0.256	0.204	3.750

According to the ISO 187, all samples were pre-treated for periods exceeding 48 h at 23 ± 1°C and 50 ± 2% relative humidity, and the experimental environment was maintained under the same temperature and humidity conditions.

The base paper tension test can obtain the tensile load-displacement data and convert it into a stress-strain curve to obtain the ultimate stress of the corrugated board base paper, which can be used to calculate the flow stress. The corresponding parameter values are provided for the calculation of the theoretical value of the plateau stress of the corrugated fibreboard.

The experiment was carried out using the Electromechanical universal testing machine (Fig. 13a). According to ISO 1924-2, the size of the corrugated fibreboard sample was 12.7 mm × 152 mm, the distance between fixtures was 60 mm, and the loading speed was 1 ± 0.2 mm·min^{-1}. Ten repetitions of the test were conducted.

A quasi-static edgewise crushing test of the corrugated fibreboard was conducted to determine the plateau stress (Fig. 13b). The experiment was conducted using the Electromechanical universal testing machine. According to ISO 3037, the size of the corrugated fibreboard sample was 25 mm × 100 mm, the loading speed was 12.5 ± 2.5 mm·min^{-1}, and the end strain was set to 85%. Five repetitions of the test were conducted.

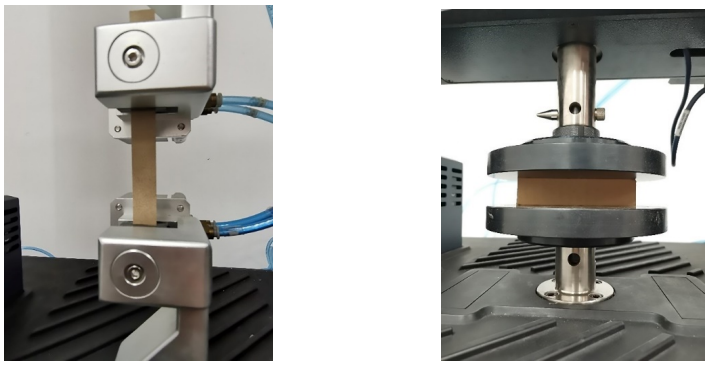

(a) (b)

Fig. 13: (a) Tension test of the base paper, (b) quasi-static compression test of corrugated fibreboard.

RESULTS AND DISCUSSION

The tensile stress-strain curve of the corrugated paper (230/130/150-C) is illustrated in Fig. 14. The ultimate stresses of the linerboard Ⅰ, the fluted board, and linerboard Ⅱ, as obtained from this curve, are listed in Tab. 2. The stress-strain curves of specimens 1–5 of the corrugated fibreboard (230/130/150-C) under quasi-static edgewise compression are presented in Fig. 15. The plateau stresses of the three types of corrugated fibreboards were identified, and they are listed in Tabs. 3–5. The experimental results indicated that the numbers of folding elements in the outer and inner folding modes were small. By contrast, the asymmetric deformation accounted for the vast majority of elements.

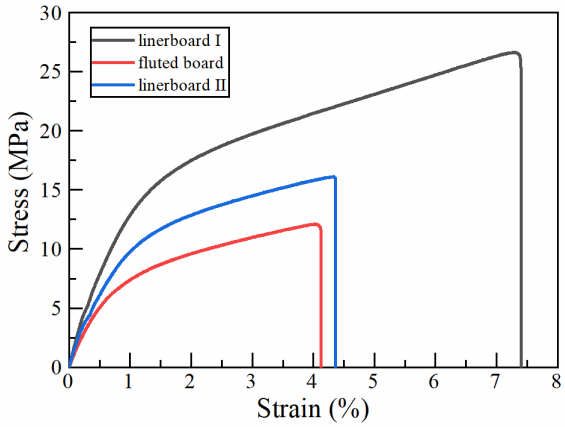

Fig. 14: Tensile stress-strain curve of corrugated papers.

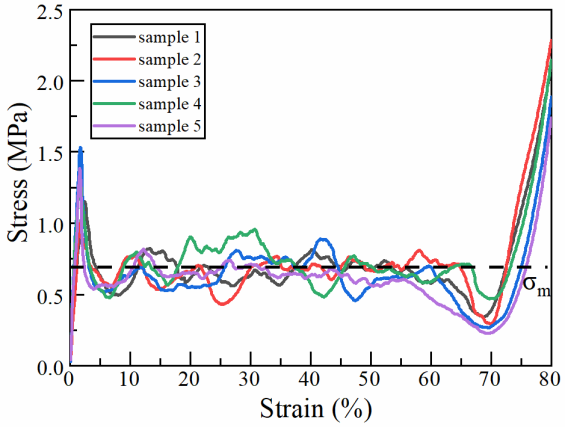

Fig. 15: Stress-strain curves of theory and experiment of corrugated fibreboard.

Tab. 2: Parameters in the experimental stress-strain curves of corrugated papers.

Specimens	Ration ($g \cdot m^{-2}$)	The ultimate stress of linerboard (MPa)	The ultimate stress of fluted board (MPa)	The ultimate stress of linerboard Ⅱ (MPa)
A	120/110/120	14.0	11.1	14.0
C	170/160/170	29.5	10.9	29.5
C	230/130/150	26.4	12.0	16.3

Based on test results, assuming that the ratio coefficient of asymmetric mode accounted for the entire proportion of the folding mode, the values of x, y, and z were set to 1, 0, and 0, respectively. Thus far, all parameters in Eq. 27 can be obtained, except for k. Several researchers have provided an arbitrary value of k within the range 0.70–0.75 (Chen and Wierzbicki 2001, Kim 2002), so value k was assumed to be constant at 0.70 for all central angles.

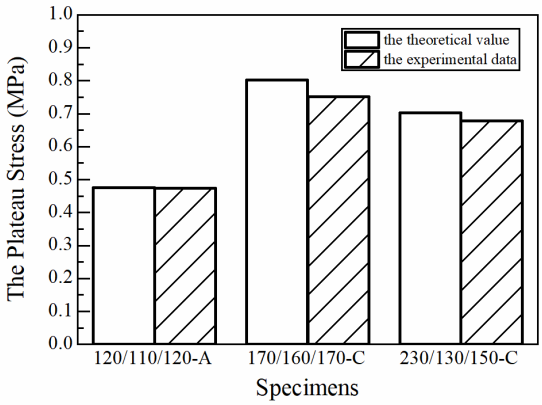

Fig. 16: The experimental data and theoretical value of the plateau stress.

The theoretical prediction results of the single-wall corrugated fibreboards under quasi-static edgewise crushing were obtained by substituting the corresponding parameters into Eq. 27. The plateau stress of the corrugated paper board, as calculated using Eq. 27, was compared to the experimentally obtained values, as summarized in Tabs. 3–5 and illustrated in Fig. 16; the comparison revealed high levels of consistency between the two sets of values.

Tab. 3: Difference between experimental data and theoretical value of corrugated fibreboard (120/110/120-A).

Specimens	Theoretical plateau stress (MPa)	Experimental plateau stress (MPa)	Relative error (%)
1	0.475	0.489	2.947
2		0.484	1.895
3		0.449	5.474
4		0.483	1.684
5		0.463	2.526
Average		0.474	2.905

Tab. 4: Difference between experimental data and theoretical value of corrugated fibreboard (170/160/170-C).

Specimens	Theoretical plateau stress (MPa)	Experimental plateau stress (MPa)	Relative error (%)
1	0.802	0.820	2.244
2		0.686	14.464
3		0.680	15.212
4		0.739	7.855
5		0.834	3.990
Average		0.752	8.770

Tab. 5: Difference between experimental data and theoretical value of corrugated fibreboard (230/130/150-C).

Specimens	Theoretical plateau stress (MPa)	Experimental plateau stress (MPa)	Relative error (%)
1	0.702	0.669	4.701
2		0.668	4.843
3		0.685	2.422
4		0.711	1.282
5		0.658	6.268
Average		0.678	3.902

The theoretically predicted and experimental values of the three types of corrugated fibreboards are summarized in Tabs. 3–5. It can be seen that the range of relative error was 1.282–15.212%, and the average error was less than 8.77%, which is between the theoretical and experimental values of the three types of corrugated fibreboards. The theoretical prediction results were consistent with the experimental values, which proved the accuracy of the proposed trapezoidal theoretical model. In other words, surface bonding is an important factor that cannot be ignored in the process of simplifying corrugated fibreboard models.

CONCLUSION

In this paper, a physical surface bonding was assumed to represent the interaction between the fluted board and the linerboard of corrugated fibreboard. Then, a new typical folding element of single-wall corrugated fibreboards and three deformation modes of the fluted board were proposed. The results indicated that local perturbations in the deformation pattern

of the linerboard were related to three different folding modes of the core, and the mapping of the crushing force obtained using a unit-cell model depended on the local deformation mode. Moreover, a plateau stress model was formulated and characterized using the structure factors of the corrugated cell wall. A comparison between the theoretical and experimental results indicated high levels of consistency between the two sets. This work has advanced the theoretical research of corrugated fibreboards under edgewise crushing load, and the proposed theoretical model provides a theoretical basis for selecting the paper for corrugated fibreboards by considering the appropriate parameters. Notably, the model of multi-wall corrugated fibreboard under edgewise crushing load warrants further development.

ACKNOWLEDGEMENTS

The authors would like to appreciate the support from the Natural Science Foundation of Jiangsu Province, China (Grant No. BK20151128), National First-Class Discipline Program of Light Industry Technology and Engineering (LITE2018-29), the 111 Project (No. B18027), and Natural Science Foundation of Zhejiang Province (Grant number: LY16A020004).

REFERENCES

1. Aboura, Z., Talbi, N., Allaoui, S., Benzeggagh, M.L., 2004: Elastic behavior of corrugated cardboard: experiments and modeling. Composite Structures 63(1): 53-62.
2. Abramowitz, W., Wierzbicki, T., 1989: Axial crushing of multi corner sheet metal columns. International Journal of Applied Mechanics 56: 113–20.
3. Bai, J., Wang, J., Pan, L., Lu, L.X., Lu, G.X., 2019: Quasi-static axial crushing of single wall corrugated paperboard. Composite Structures 226: 111237.
4. Buannic, N., Cartraud, P., Quesnel, T., 2003: Homogenization of corrugated core sandwich panels. Composite Structures 59(3): 299-312.
5. Chen, W., Wierzbicki, T., 2001: Relative merits of single-cell, multi-cell and foam-filled thin-walled structures in energy absorption. Thin-Walled Structures 39(4): 287-306.
6. Duan, L.B., Du, Z.P., Jiang, H.B., Xu, W., Li, Z.J., 2019: Theoretical prediction and crashworthiness optimization of top-hat thin-walled structures under transverse loading. Thin-Walled Structures 144: 106261.
7. Fan, Z., Lu, G., Yu, T.X., Liu, K., 2013: Axial crushing of triangular tubes. International Journal of Applied Mechanics 05(01): 1350008.
8. Gao, Q., Liao W.H., 2021: Energy absorption of thin walled tube filled with gradient auxetic structures - theory and simulation. International Journal of Mechanical Sciences 201: 106475.
9. Garbowski, T., Gajewski, T., Grabski, J.K., 2021: Estimation of the compressive strength of corrugated cardboard boxes with various perforations. Energies 14(4): 1095
10. Isaksson, P., Krusper, A., Gradin, P.A., 2007: Shear correction factors for corrugated core structures. Composite Structures 80(1): 123-130.

11. ISO 187, 1990: Standard: Paper, board and pulp. Standard atmosphere for conditioning and testing and procedure for monitoring the atmosphere and conditioning of samples.
12. ISO 1924-2, 2008: Standard: Paper and board. Determination of tensile properties.
13. ISO 3037, 2013: Standard: Corrugated fiberboard. Determination of edgewise crush resistance.
14. Jamsari, M., Kueh, C., Gray-Stuart, E.M., Dahm, K., Bronlund, J.E., 2020: Modelling the impact of crushing on the strength performance of corrugated fiberboard. Packaging Technology and Science 33(4-5): 159-170.
15. Kim, H.S., 2002: New extruded multi-cell aluminum profile for maximum crash energy absorption and weight efficiency. Thin-Walled Structure 40: 311–27.
16. Kolakowski, Z., Szewczyk, W., Glowacki, K., 2015: Calculation of corrugated board flat crush resistance. Wood Research 60(5): 747-754.
17. Li, X, Wang, J., Huang, C.X., Gao, D., Lu, G.X., Lu, L.X., Wang, Z.W., 2018: Mathematical models for predicting the quasi-static stress characteristics of corrugated paperboard with sinusoidal core along the longitudinal compression. International Journal of Mechanical Sciences 149: 136-149.
18. Moon, J., Yi, J., Choi, B.H., Lee, H.E., 2009: Shear strength and design of trapezoidally corrugated steel webs. Journal of Constructional Steel Research 65(5): 1195-1205.
19. Russ, A., Schwartz, J., Bohacek, S., Lubke, H., Ihnat, V., Pazitny, A., 2013: Reuse of old corrugated cardboard in constructional and thermal insulating boards. Wood Research 58(3): 505-510
20. Szewczyk, W., Bienkowska, M., 2020: Effect of corrugated board structure on mechanical properties. Wood Research 65(4): 653-662.
21. Urbanik, T.J., 2001: Effects of corrugated flute shape on fiber board edgewise crush strength and bending stiffness. Journal of Pulp and Paper Science 27(10): 330-335.
22. Wang, Z., Liu, J., Yao, S., 2018: On folding mechanics of multi-cell thin-walled square tubes. Composites Part B: Engineering 132: 17-27.
23. Westerlind, B.S., Carlsson, L.A., 1992: Compressive response of corrugated board. Tappi Journal 75(7): 145-154.
24. Wierzbicki, T., 1983: Crushing analysis of metal honeycombs. Impact Engineering 1(2): 157-174.
25. Yu-Ping, E., Wang, Z.W., 2012: Stress plateau of multilayered corrugated paperboard in various ambient humidities. Packaging Technology and Science 25(4): 187-202.
26. Zhang, X., Zhang, H., 2013: Theoretical and numerical investigation on the crush resistance of rhombic and kagome honeycombs. Composite Structures 96: 143-152.
27. Zhang, Z., Lei, H.S., Xu, M.C., Hua, J., Li, C.L., Fang, D.N., 2019: Out-of-plane compressive performance and energy absorption of multi-layer graded sinusoidal corrugated sandwich panels. Materials & Design 178: 107858.

GUAN SHILI, LIANG YOUZHEN, WANG JUN*, LU LIXIN
JIANGNAN UNIVERSITY
JIANGSU KEY LABORATORY OF ADVANCED FOOD MANUFACTURING EQUIPMENT AND TECHNOLOGY, DEPARTMENT OF PACKAGING ENGINEERING
1800 LI HU AVENUE
WUXI, CHINA
*Corresponding author: wangj_1982@jiangnan.edu.cn

HOU XUE
WUXI INNOVATION RESEARCH INSTITUTE OF SHANTOU DONGFENG PRINTING CORPORATION
WUXI, NO.8 FINANCE STREET
CHINA